Supporting information

for

Electric rectification by a Redox-Conductive Metal-Organic Framework Bilayer Electrode

Li, Jingguo[1,2], Kumar, Amol[1*,] Ott, Sascha[1*]

1 Department of Chemistry – Ångström Laboratory, Uppsala University, Box 523, 75237 Uppsala, Sweden

2 State Key Laboratory of Advanced Environmental Technology, Department of Environmental Science and Engineering, University of Science and Technology of China, Hefei 230026, China

* Corresponding authors: amol.kumar@kemi.uu.se; Sascha.Ott@kemi.uu.se

Table of Contents

General information: Materials and Instrumentation

Materials

All solvents and commercially supplied chemicals were reagent grade and used as received without further purification, unless stated otherwise. $Zn(NO_3)_2 \cdot 6H_2O$ was purchased from Sigma-Aldrich, benzene-1,2,4,5-tetracarboxylic dianhydride (≥99.0%) from Sigma-Aldrich naphthalene-1,4,5,8-tetracarboxylic dianhydride (≥97.0%) from TCI, 4-amino-3,5-dimethylpyrazole (≥95.0%) from Doug Discovery $[Co(bpy)_3](PF_6)_3$ (bpy = 2,2′-bipyridyl) was obtained from TCI Chemicals and N, N-dimethylformamide (DMF) (99.9%) from VWR. Potassium hexafluorophosphate (KPF_6, for electrochemical analysis, ≥99.0%) and fluorine-doped tin oxide (FTO) substrates (7 Ω/sq) were purchased from Sigma-Aldrich.

Instrumentation

Nuclear Magnetic Resonance (NMR): ^{1}H NMR spectra were recorded on a JEOL 400 MHz spectrometer at 293 K. Proton chemical shifts are expressed in parts per million (δ scale) and are calibrated using residual non-deuterated solvent peaks as an internal reference (^{1}H NMR: $CDCl_3$: 7.26, DMSO-d6: 2.50). Data for ^{1}H NMR spectra are reported in the following way: chemical shift (δ ppm) (multiplicity, integration).

Scanning Electron Microscopy (SEM): Scanning electron microscopy (SEM) images were obtained using a Zeiss 1550 Schottky field emission scanning electron microscope equipped with an in-lens detector operated at 1 – 30 kV acceleration voltage. MOF thin film were anchored to conductive carbon tape on a sample holder disk. Surface area and film thickness of each individual film was determined using ImageJ (NIH) software.

Powder X-Ray Diffraction (PXRD): Thin film XRD patterns were collected using a Siemens D5000 Kristalloflex equipped with a Gobel mirror (Bruker) and a parallel-plate collimator (0.40^0) using a monochromatic Cu Kα radiation (λ = 1.5406 Å) source operating at 45 kV and 40 mA. PXRD data was collected between 3 and 26^0 (2θ) range at a step size of 0.017^0.

Bilayer film formation and SEM characterization

Synthesis

The synthesis of the NDI and PMDI linkers follows previously published protocols,[1] and their purity was confirmed by ^{1}H NMR spectroscopy.

PMDI: ^{1}H NMR (400 MHz, DMSO-d6) δ ppm: 12.61 (s, 2H), 8.37 (s, 2H), 2.06 (s, 12H).
NDI: ^{1}H NMR (400 MHz, DMSO-d_6) δ ppm: 12.50 (s, 2H), 8.74 (s, 4H), 2.02 (s, 12H).

FTO slides were cut into 2.5 × 1.1 cm^2 pieces and cleaned by successive sonication in solutions of Alconox (1%), ethanol, and acetone. Prior to any film growth, a horizontal line was scratched into the FTO slide using a diamond pencil. The line isolates the bottom 15-20% of the FTO slide from the upper portion which is where all subsequent measurements are performed. This was found necessary to produce high quality data, as the bilayer electrode in the upper portion of the material exhibits more uniform coverage, minimal intermixing of the two layers or short-circuiting at the bottom edge of the FTO slide, leading to an overall improved bilayer performance (Bottom part of the film was thinner compared to rest of the top film due to steric constrains).

Bilayer FTO|Zn(NDI)|Zn(PMDI) electrode preparation: The bilayer MOF electrode was prepared through a two-step solvothermal synthesis process. First, the inner Zn(NDI) MOF thin film was grown on the surface of FTO following the previously reported procedure; a solution of $Zn(NO_3)_2 \cdot 6H_2O$ (0.11 mmol) and NDI (0.10 mmol) in DMF was prepared in a 20 mL scintillation vial and sonicated for 10 min. After deaeration with argon for 10 min, the pre-cleaned FTO slides were inserted into the reaction mixture with the FTO side facing down. The vial was sealed and placed in a gravity convection oven for 4.5 hours at 130°C. The vials were allowed to cool to room temperature, and the films were washed with DMF to remove any loosely bound powder on the surface. The unwanted growth on the glass side of the FTO was carefully removed by Kimtech wiping paper wetted with DMF. Afterwards, the second layer of Zn(PMDI) MOF was grown on top of the Zn(NDI) film by a secondary solvothermal synthesis; where a solution of $Zn(NO_3)_2 \cdot 6H_2O$ (0.11 mmol) and PMDI (0.10 mmol) in DMF was used. This time, previously grown FTO|Zn(NDI) was inserted into the reaction mixture with the FTO|Zn(NDI) side facing down. The vial is then kept in the oven for another 4.5 hours at 130°C, followed by a similar washing procedure. The final FTO|Zn(NDI)|Zn(PMDI) bilayer electrode were then soaked in DMF until further use.

The reverse geometry FTO|Zn(PMDI)|Zn(NDI) bilayer electrode was prepared following a similar two-step solvothermal synthesis with Zn(PMDI) as inner and Zn(NDI) as outer layer.

SEM characterization

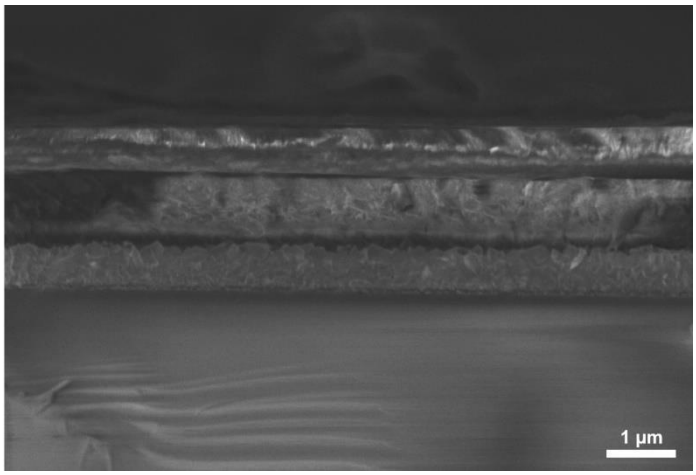

Figure S1. SEM cross-section image of a FTO|Zn(PMDI)|Zn(NDI) electrode.

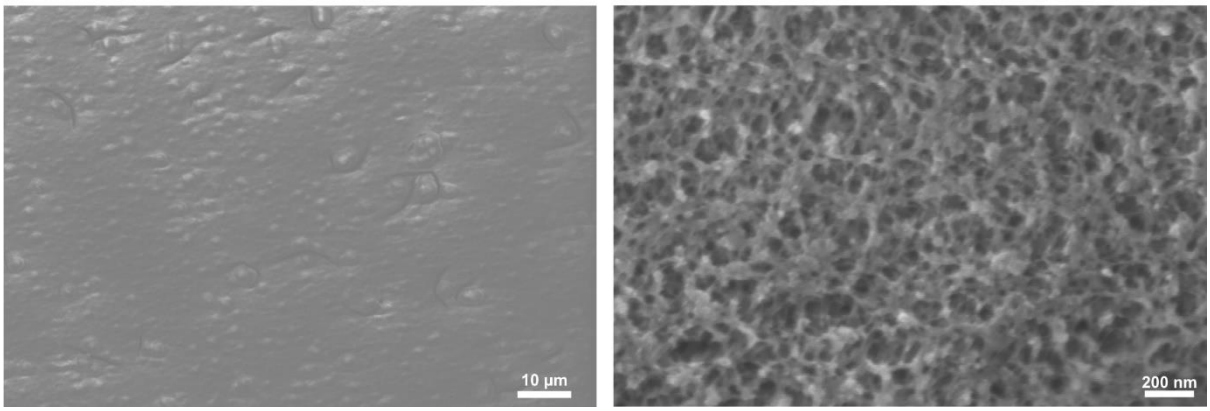

Figure S2. SEM top surface images of FTO|Zn(NDI)|Zn(PMDI) electrode at different magnification.

Cyclic Voltammetry

Electrochemical analyses were performed in a standard three-electrode set-up connected to an Autolab PGSTAT204 potentiostat controlled with Nova 2.1.4 software: the bilayer electrodes FTO|Zn(NDI)|Zn(PMDI) and FTO|Zn(PMDI)|Zn(NDI) were used as the working electrode, a glassy carbon as the counter electrode, and a non-aqueous Ag/Ag^+ reference electrode (10 mM $AgPF_6$ in acetonitrile). Prior to measurements, all electrodes were washed carefully to remove loosely bound partials and the glass side of the substrate was wiped with Kimwipe (KIMTECH) to remove any MOF growth on the glass side. The electrodes were then kept in fresh DMF solvent for subsequent/future experiments. A solution of 0.5M KPF_6 in dry DMF was used as the supporting electrolyte and degassed for 10 min by argon bubbling before each experiment. During measurements, the headspace of the electrochemical cell was continuously purged with argon. The electrolytes were directly used as bought and the solvent was taken from the solvent purification system (SPS) without any further purification. The applied potentials were calibrated against the $Fc^{+/0}$ redox couple, which was added after each experiment as an internal standard.

Because the MOF is immobilized and the concentration of electroactive units is constant over forward and reverse potential sweeps in a CV experiment, the shape of the current response and the area under the cathodic and anodic peak give information about chemical reversibility. Unlike a freely diffusing analyte, where an electrochemically reversible redox pair typically exhibits a peak separation of 57 mV, surface immobilized MOFs often show variable peak separation. These can range from close-to-zero at very low scan rates to a significantly larger value at high scan rates, depending on the charge transport kinetics of the MOF.

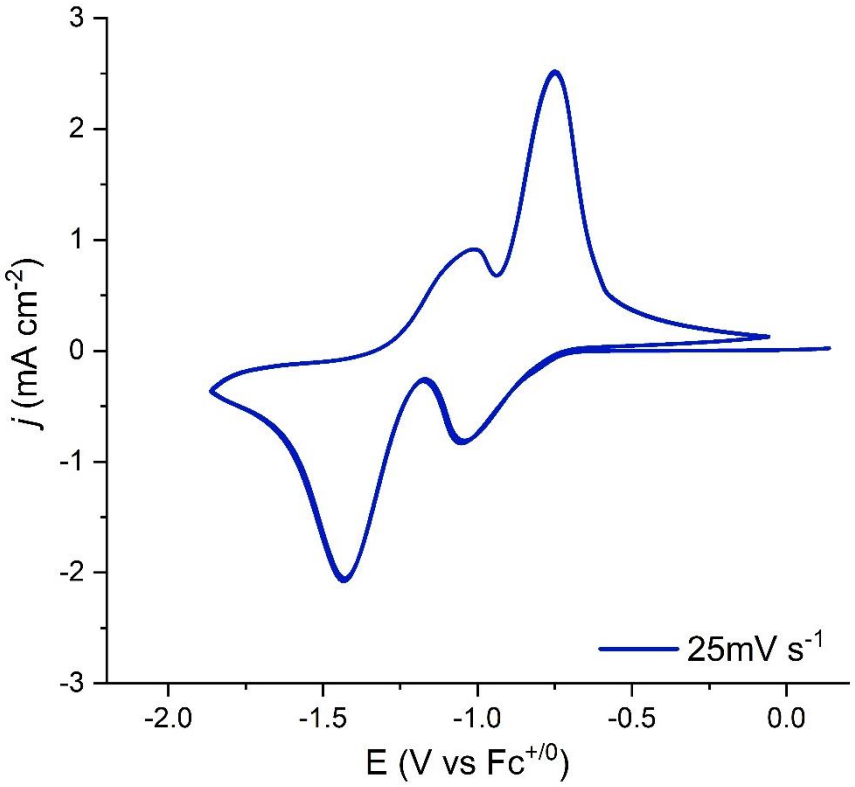

Figure S3. Cyclic voltammogram of FTO|Zn(NDI)|Zn(PMDI) in Ar-saturated DMF with KPF_6 as the supporting electrolyte (0.5 M) at scan rates from 25 mV s^{-1} (3 consecutive scans).

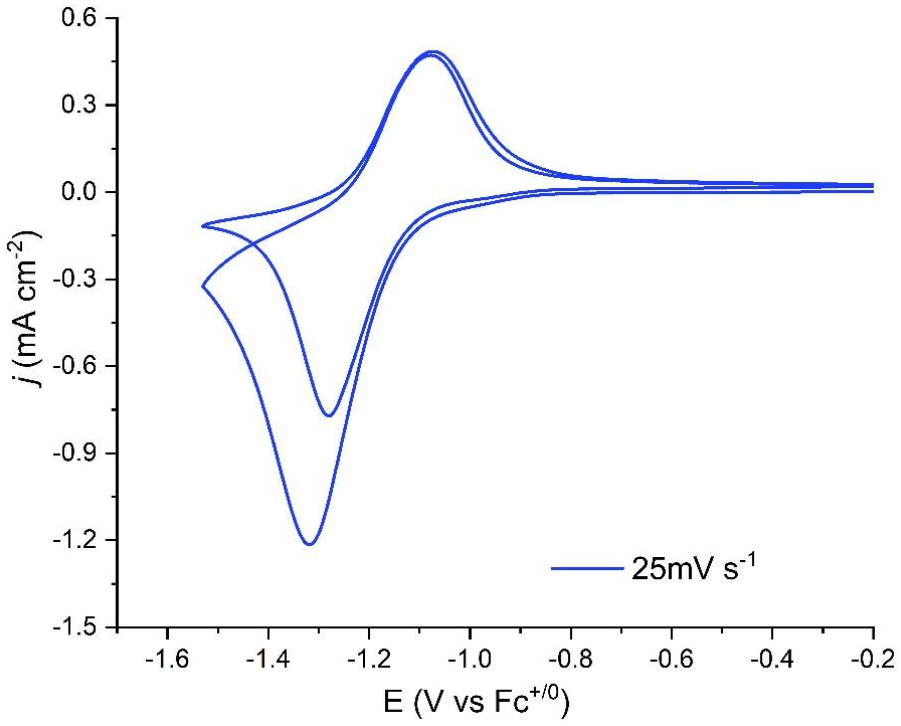

Figure S4. Cyclic voltammogram of FTO|Zn(PMDI)|Zn(NDI) (only first reduction) in Ar-saturated DMF with KPF_6 as the supporting electrolyte (0.5 M) at scan rates from 25 mV s^{-1}.

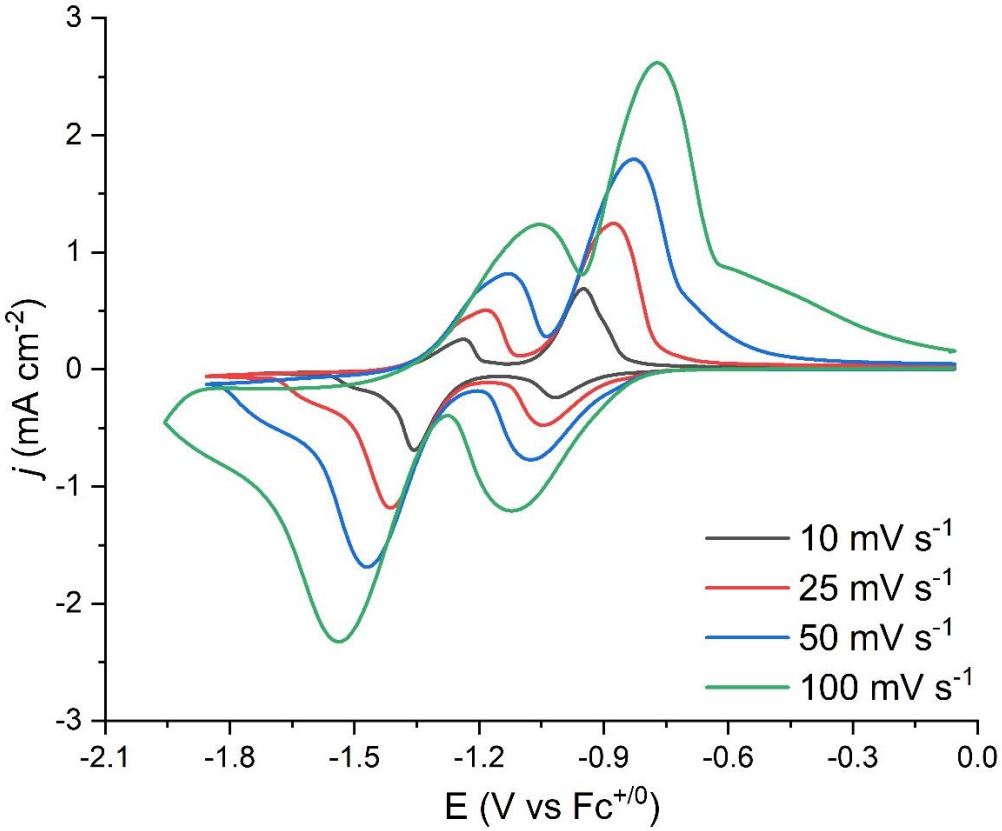

Figure S5. Scan-rate-dependent cyclic voltammograms of FTO|Zn(NDI)|Zn(PMDI). All CV data were collected in Ar-saturated DMF with KPF_6 as the supporting electrolyte (0.5 M) at scan rates from 10 to 100 mV s^{-1}.

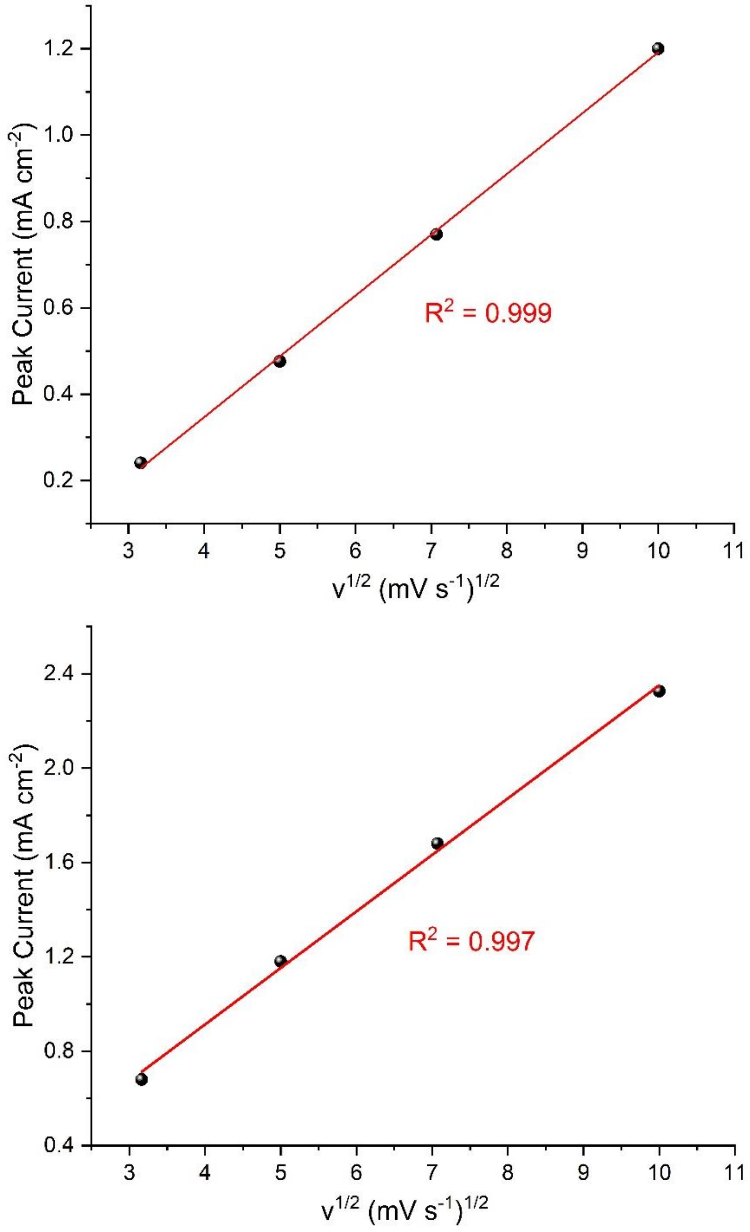

Figure S6. Plot of cathodic peak currents with square root of scan rate ($v^{-1/2}$) corresponding to 1st direct reduction $NDI^{0/\bullet-}$ (top) and, 2nd Mediated reduction of $PMDI^{0/\bullet-}$ through $NDI^{\bullet-/2-}$ (bottom). The straight lines are characteristic of the diffusional electron hopping transport through the electrode.

Spectroelectrochemistry

Time-resolved UV–Vis spectra of electrogenerated species were collected *in operando* using a diode array spectrophotometer (Agilent 8453) coupled to an Autolab PGSTAT100 potentiostat controlled by NOVA 2.1.4 software. The bilayer electrodes as well as the mixed-linker FTO|Zn(PMDI)$_{0.5}$(NDI)$_{0.5}$ electrode were used as working electrodes in a single-compartment electrochemical cell consisting of a quartz cuvette with a 1 cm optical pathlength, with a Pt rod counter electrode, and a non-aqueous Ag/Ag^{+} reference electrode (10 mM $AgPF_6$ in acetonitrile). The cell was equipped with a home-made stopper holding three electrodes (Fig. S7). Only the working electrode was positioned in the optical path to minimize spectral interference and all other components remain outside the optical path. Spectroscopic background spectra were acquired using bare FTO substrates immersed in the same electrolyte under identical conditions. To assign the electrochemical events in the bilayer MOFs, absorption spectra were collected in kinetic mode simultaneously with electrochemical operation, including CV measurements of each electrode, enabling real-time monitoring of electrogenerated species. All SEC experiments were performed under an argon atmosphere to exclude oxygen, and electrolyte solutions were degassed prior to measurements. Identical conditions were maintained for background and sample measurements to ensure reliable subtraction of FTO and solvent contributions. This setup enabled selective monitoring of closely spaced redox events in FTO|Zn(PMDI)$_{0.5}$(NDI)$_{0.5}$ with distinct absorption profile for each reduction step (Fig. S8) and mapping concerted reduction processes for the bilayer electrodes to be distinguished through monitoring evolution and decay of their distinct absorption profile (Fig. S9).

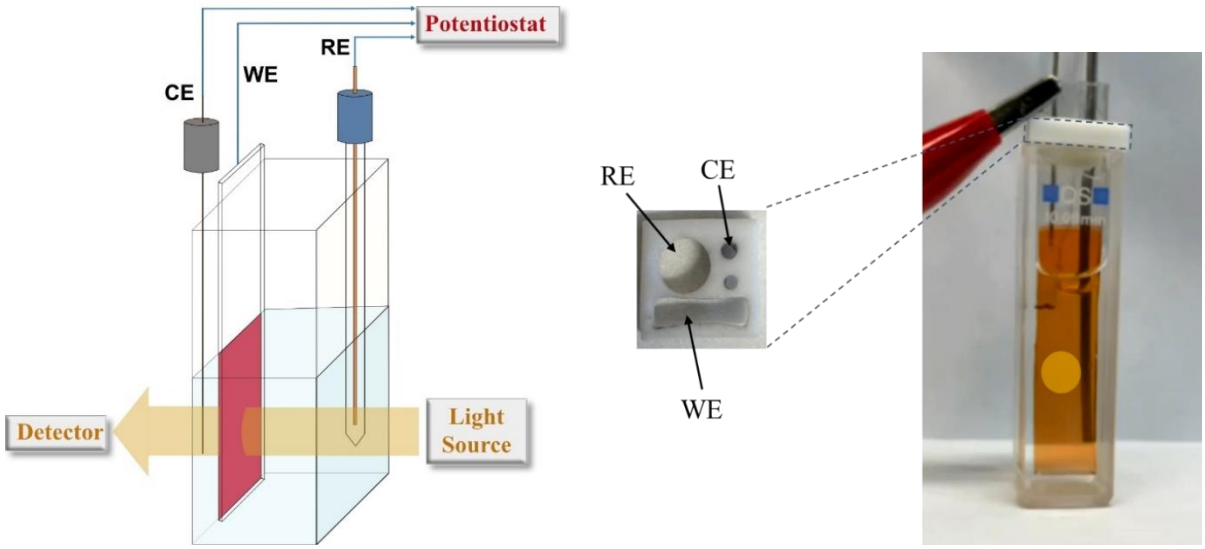

Figure S7. Schematic representation and real-world picture of the experimental set-up: the 3-electrode quartz cell for the spectroelectrochemical analysis of the electrodes as working electrode, Pt as counter, and $Ag/AgNO_3$ as reference electrode.

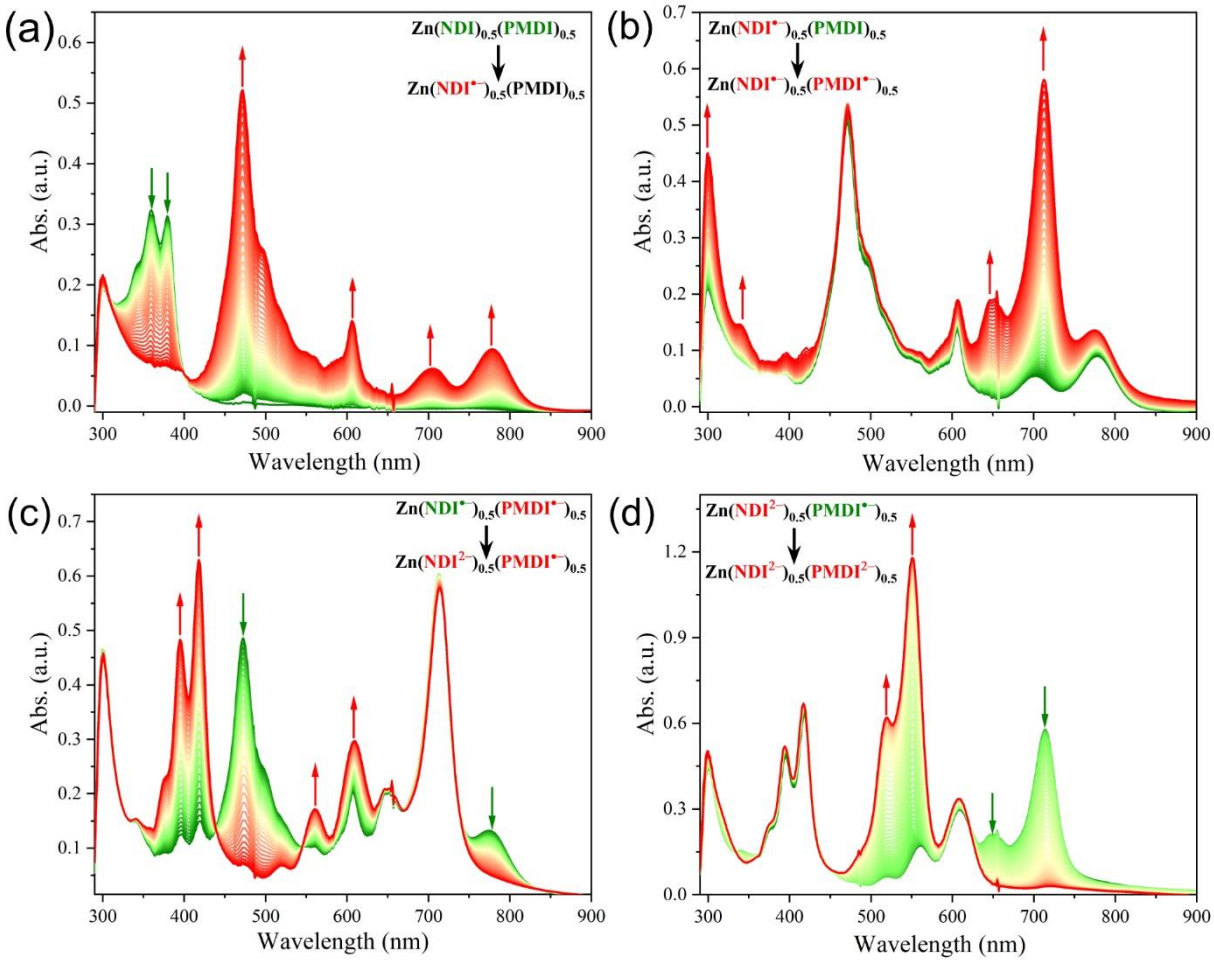

Figure S8. Operando UV-vis measurements of FTO|$Zn(PMDI)_{0.5}(NDI)_{0.5}$ while running the CV at slow scan rate of 10 mV/s. In the mixed-linker MOF, all redox couples are in direct contact to the FTO electrode and, consequently, the material can be prepared in a total of five oxidation states (from neutral to FTO|$Zn(PMDI^{2-})_{0.5}(NDI^{2-})_{0.5}$). The individual transformations are described in the Figure. All redox states are characterized by distinct UV/Vis signatures. a) singly reduced radical state $Zn(NDI^{\bullet-})_{0.5}(PMDI)_{0.5}$, obtained during the CV scan between –0.9 V and –1.1 V. b) Doubly reduced mixed radical state $Zn(NDI^{\bullet-})_{0.5}(PMDI^{\bullet-})_{0.5}$, obtained during the CV scan between – 1.15 V and – 1.25 V. c) Triply reduced mixed radical-dianion state $Zn(NDI^{2-})_{0.5}(PMDI^{\bullet-})_{0.5}$, obtained during the CV scan between – 1.3 V and – 1.4 V. d) 4-fold reduced mixed dianion state $Zn(NDI^{2-})_{0.5}(PMDI^{2-})_{0.5}$, obtained during the CV scan between – 1.55 V and – 1.65 V.

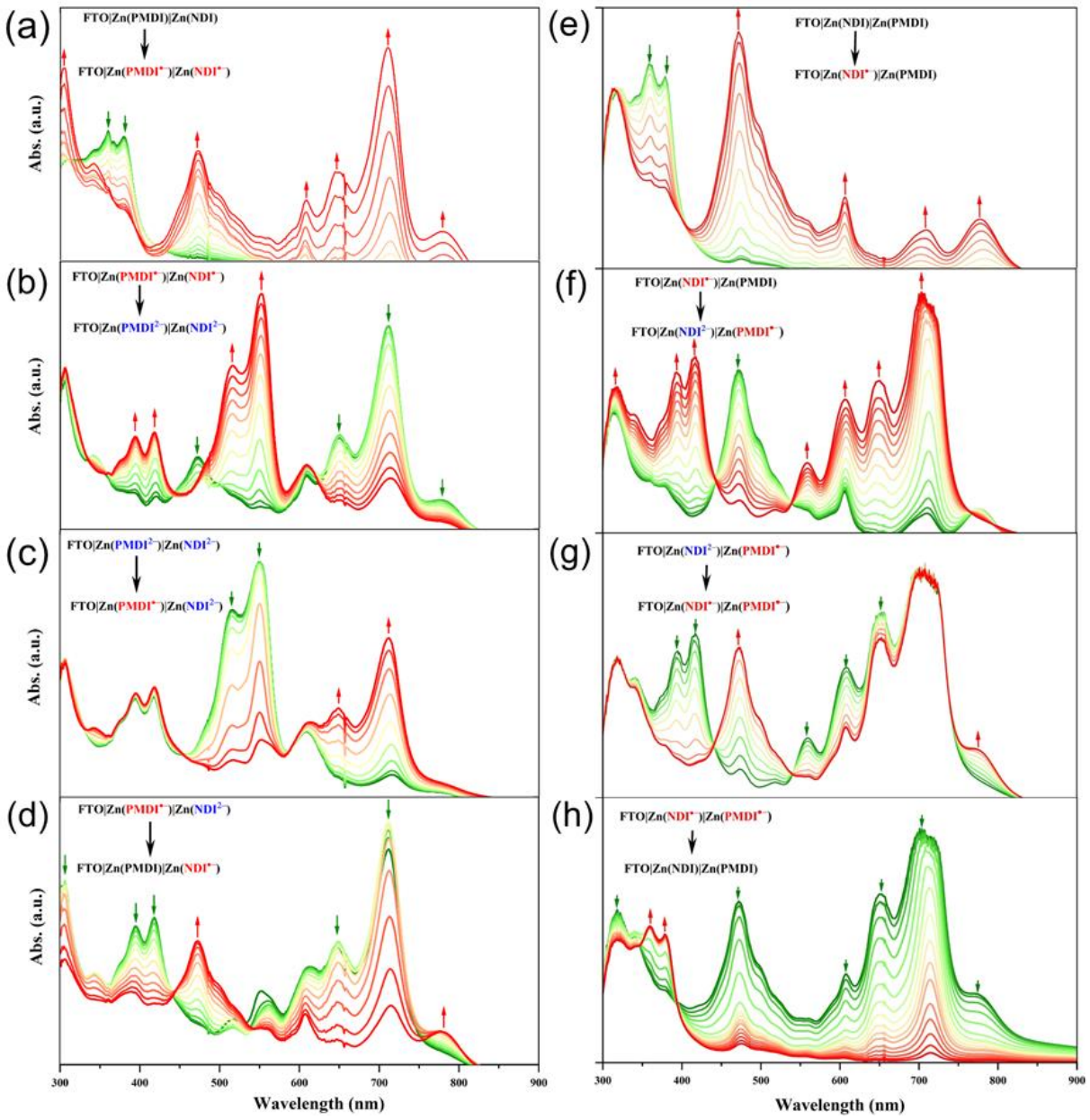

Figure S9. UV-vis spectroscopic changes during a complete CV scan at a scan rate of 25 mV/s of the FTO|Zn(PMDI)|Zn(NDI) (a-d), and FTO|Zn(NDI)|Zn(PMDI) (e-h) bilayer electrodes. a) in the cathodic scan, the co-appearance of $PMDI^{\bullet-}$ (direct reduction) and $NDI^{\bullet-}$ (mediated reduction) at the potential of the $PMDI^{0/\bullet-}$ couple; b) subsequent reductions of both radical species; c) during the anodic reverse scan, re-oxidization of $PMDI^{2-}$, with the persistence of the NDI^{2-} state; d) re-oxidation of NDI^{2-} and $PMDI^{0/\bullet-}$, producing the $NDI^{\bullet-}$ in the Zn(NDI) outer layer after completion of the CV scan. e-h) Operando UV-vis of FTO|Zn(NDI)|Zn(PMDI) bilayer while running the CV; e) in the cathodic scan, only the $NDI^{\bullet-}$ species is observed, f) coupled appearance of NDI^{2-} (direct reduction) and $PMDI^{\bullet-}$ (mediated reduction) at the potential of the $NDI^{\bullet-/2-}$ couple. g) In the anodic reverse scan, only NDI^{2-} is re-oxidized to

$NDI^{\bullet-}$ while $PMDI^{\bullet-}$ remains unchanged; h) re-oxidation of $NDI^{\bullet-}$ (direct re-oxidation) and $PMDI^{\bullet-}$ (mediated re-oxidation) at the potential of the $NDI^{\bullet-/0}$ couple, to revert the electrode to the redox ground state.

Charge trapping in the FTO|Zn(PMDI)|Zn(NDI) bilayer electrode.

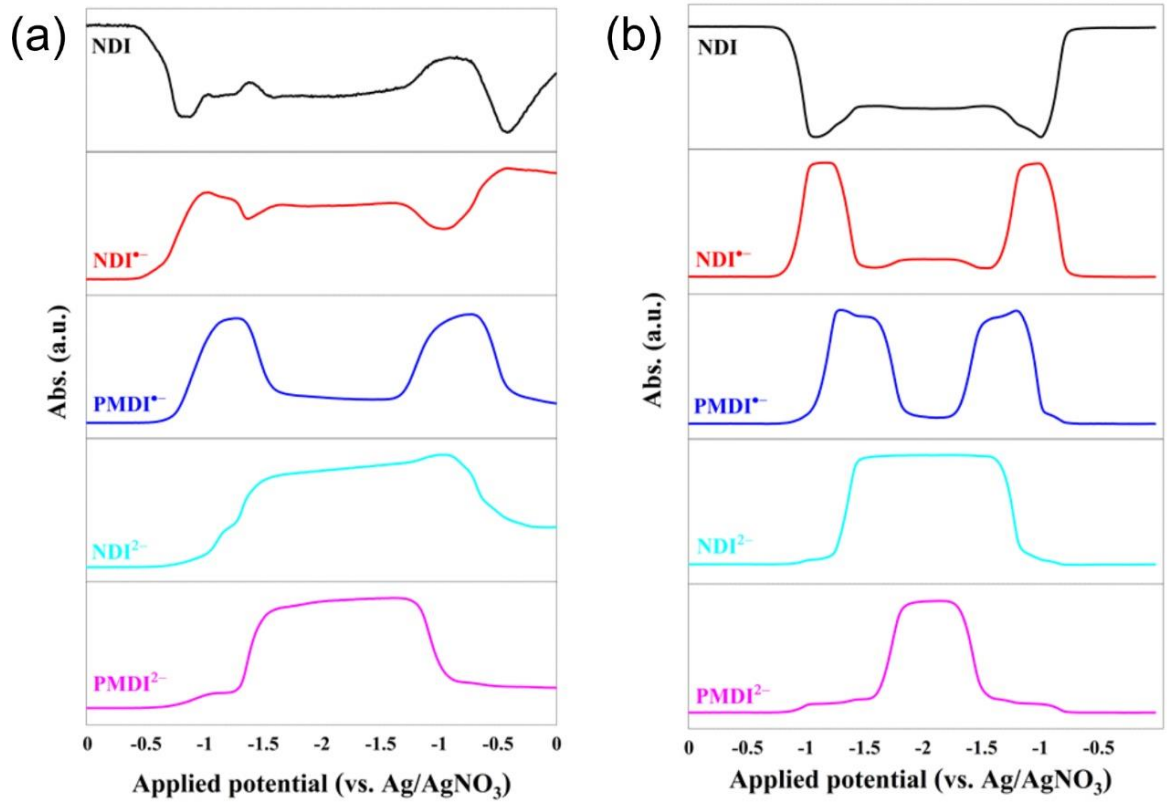

Figure S10. Evolution of the states as a function of applied potential. a) FTO|Zn(PMDI)|Zn(NDI) bilayer and b) mixed linker FTO|Zn$(PMDI)_{0.5}(NDI)_{0.5}$, following characteristic absorptions at 360 nm (NDI), 471 nm ($NDI^{\bullet-}$), 713 nm ($PMDI^{\bullet-}$), 418 nm (NDI^{2-}), and 551 nm ($PMDI^{2-}$).

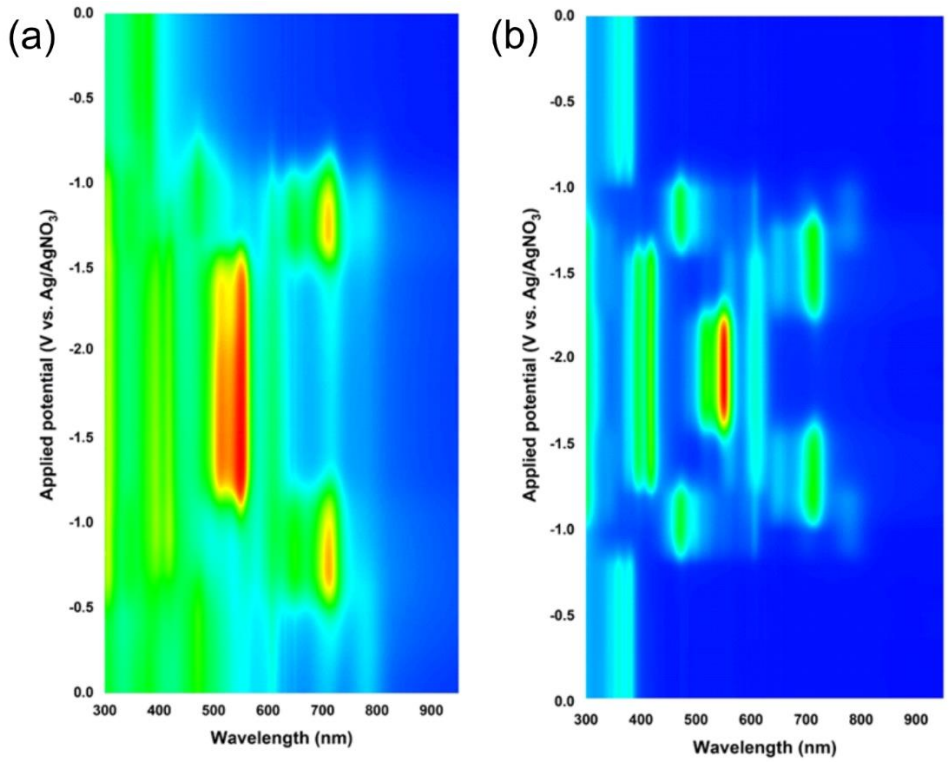

Figure S11. Contour plot of a) the FTO|Zn(PMDI)|Zn(NDI) bilayer electrode and b) the FTO|Zn(PMDI)$_{0.5}$(NDI)$_{0.5}$ film and as a function of applied potentials.

Chronoamperometry in absence and presence of acceptor ("source-drain" experiments)

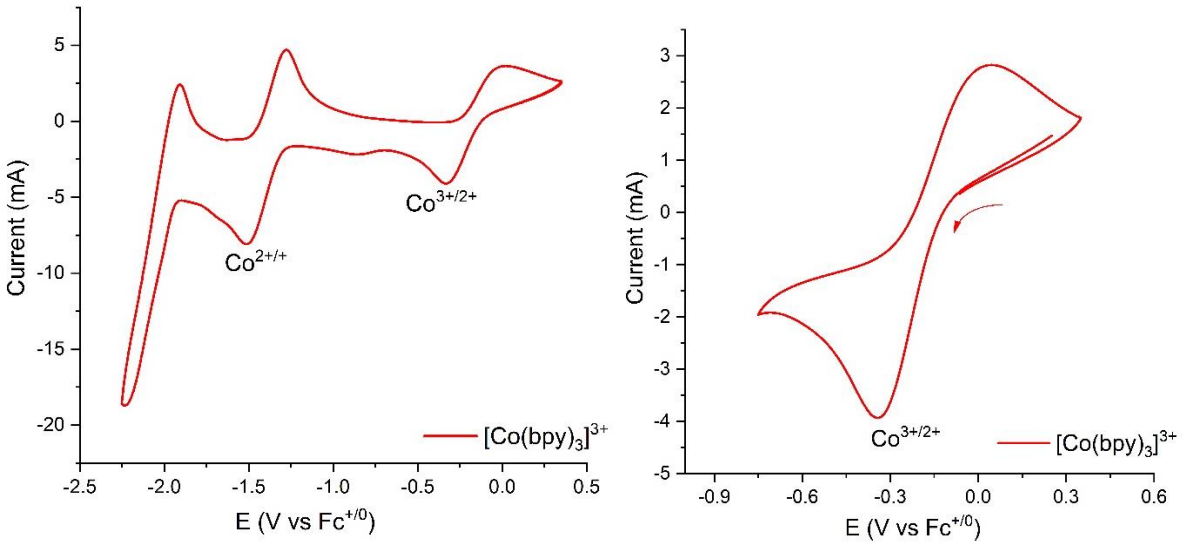

Figure S12. CV of a 1mM solution of $Co(bpy)_3]^{3+}$ in Ar-saturated DMF with KPF_6 as the supporting electrolyte (0.5 M). Glassy carbon working electrode at scan rate of 100 mV s^{-1}.

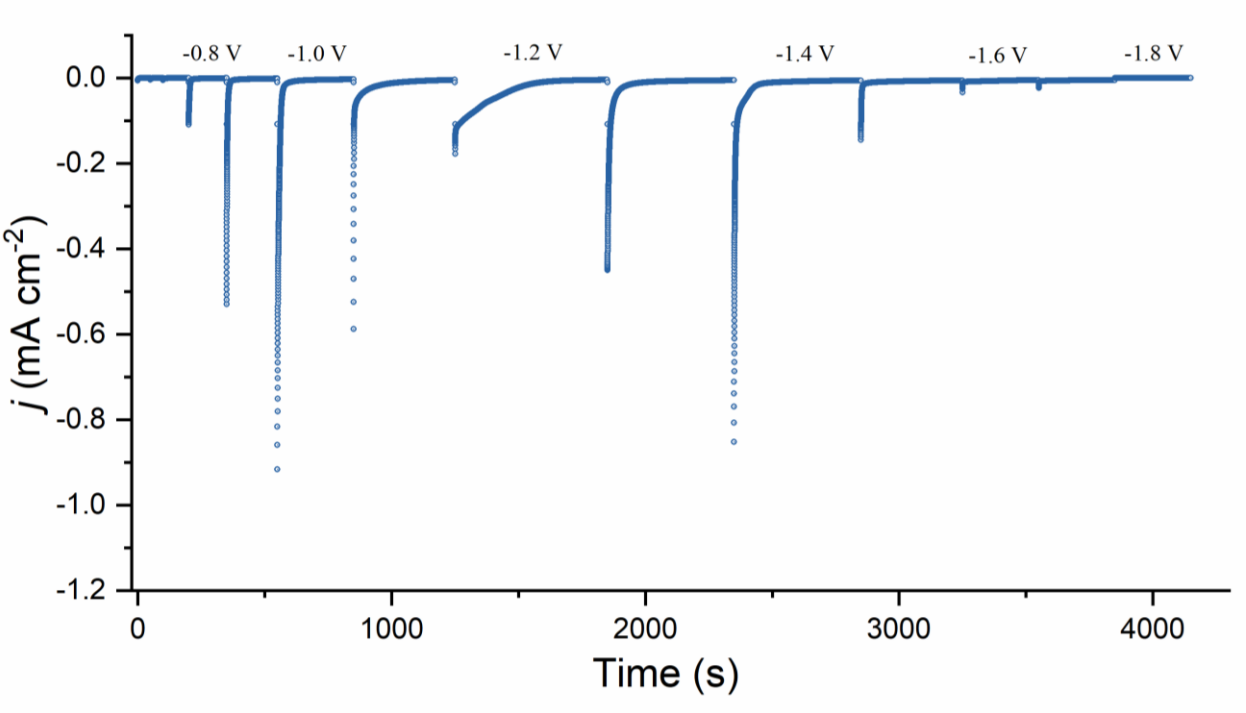

Figure S13. Steady state chronoamperometry of the FTO|Zn(NDI)|Zn(PMDI) electrode measured at different potentials in the absence of $[Co(bpy)_3]^{3+}$ in the electrolyte. The current always decays to zero once the available redox linkers are exhaustively reduced.

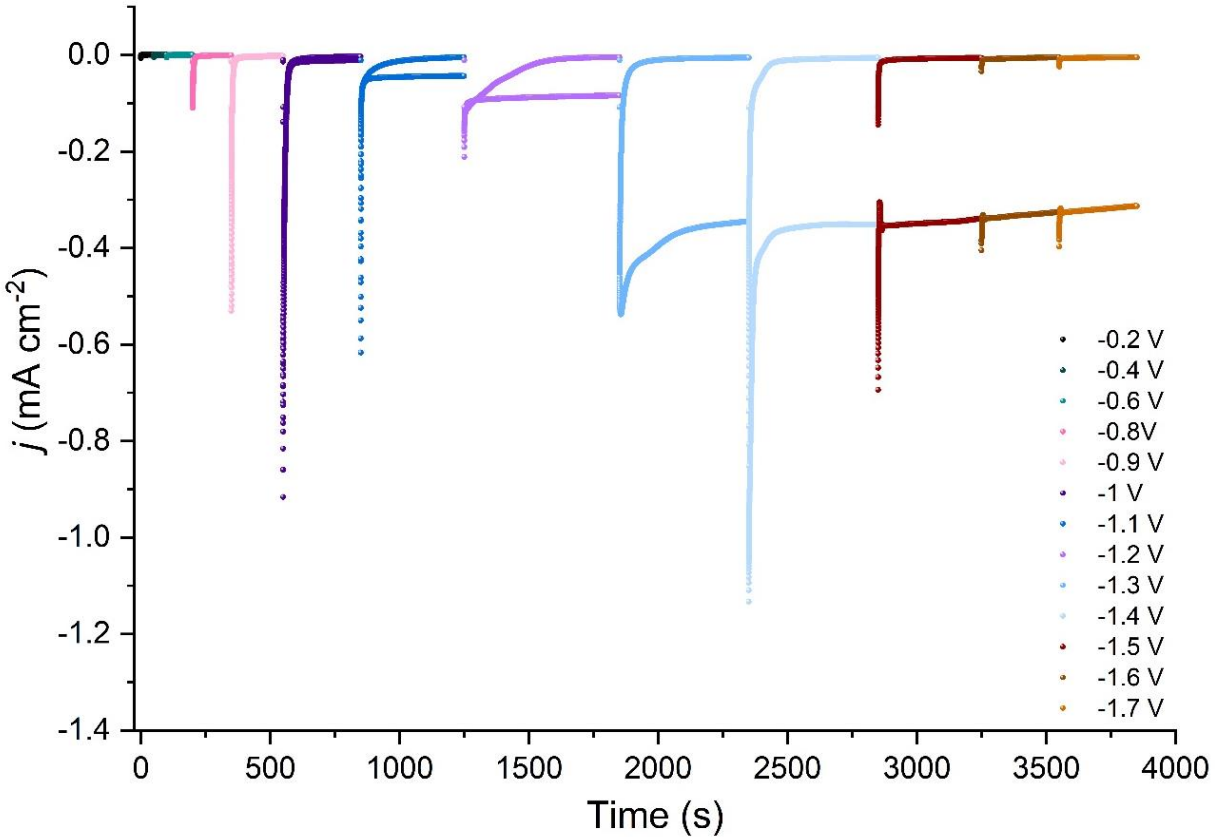

Figure S14. Steady state chronoamperometry of the FTO|Zn(NDI)|Zn(PMDI) electrode measured at different stepping potentials with and without $[Co(bpy)_3]^{3+}$ in the electrolyte. In the absence of the electron acceptor in electrolyte, the current decays to zero, while non-zero current densities are observed in the presence of $[Co(bpy)_3]^{3+}$ if the step potential is close to the $NDI^{\bullet -/2-}$ redox level.

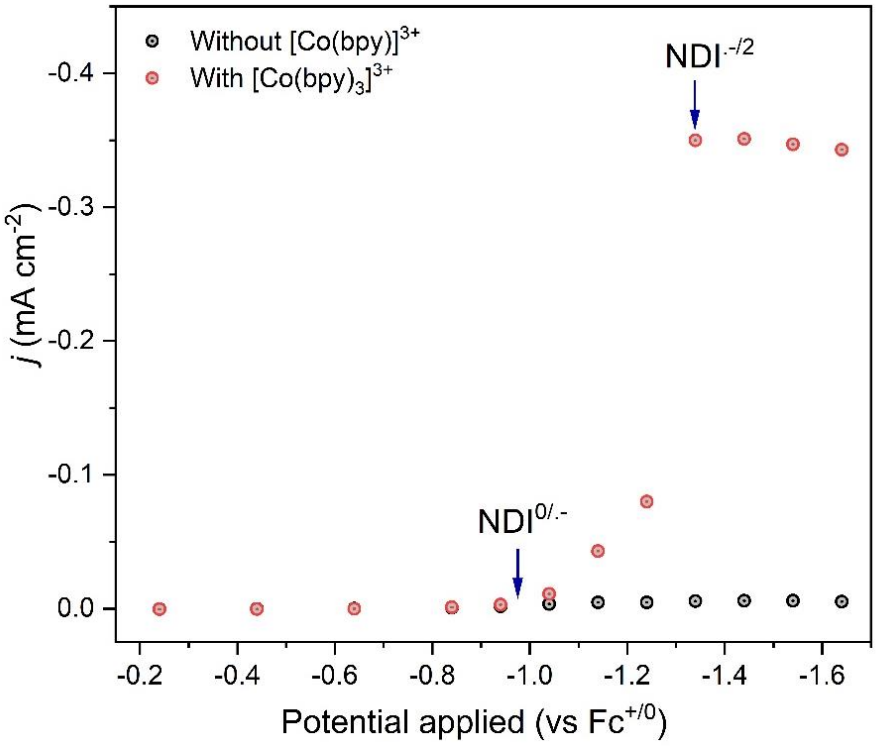

Figure S15. Steady state current densities obtained during the chronoamperometry experiments of the FTO|Zn(NDI)|Zn(PMDI) electrode in the presence of $[Co(bpy)_3]^{3+}$ in the electrolyte as a function of applied potential. The steady state current exhibits a sharp rise at the potential that corresponds to the $NDI^{\bullet -/2-}$ redox level while almost no current is observed at $NDI^{0/\bullet -}$ redox level.

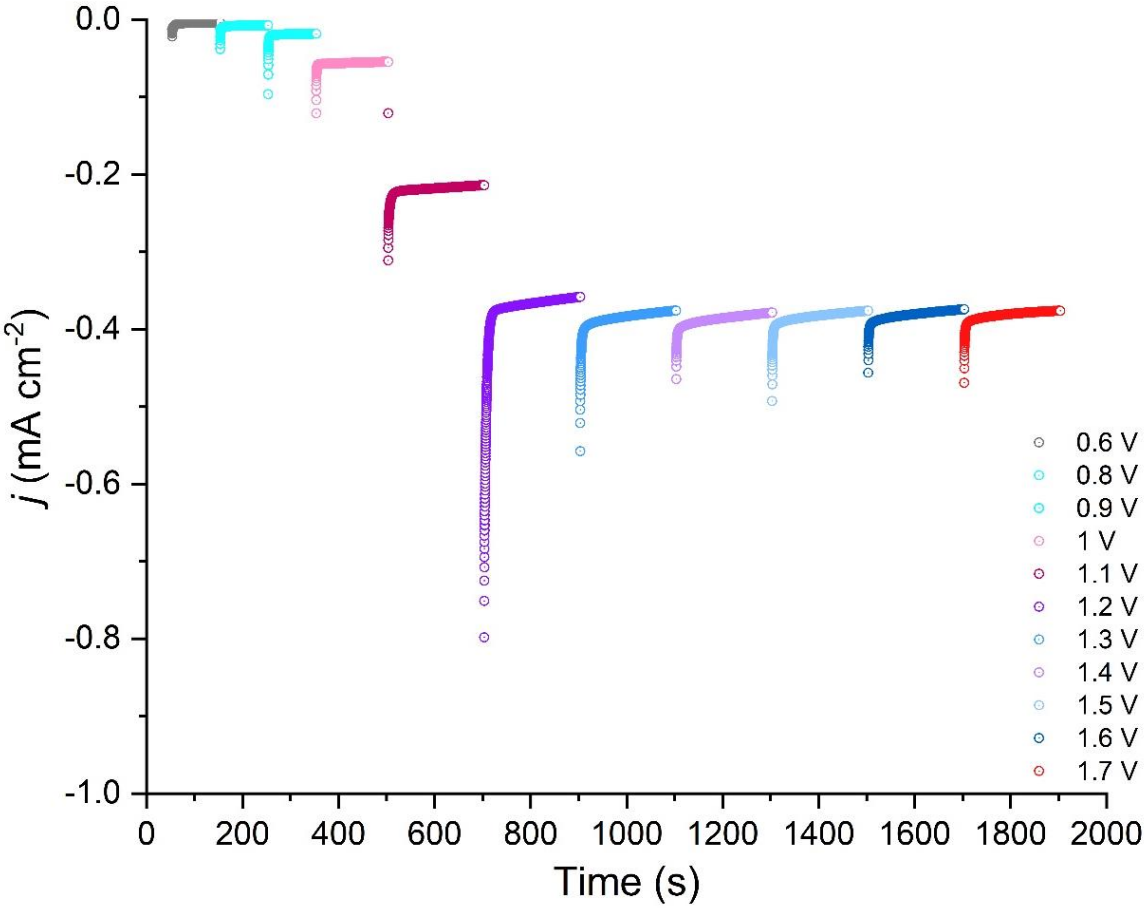

Figure S16. Chronoamperometry of the FTO|Zn(PMDI)|Zn(NDI) electrode measured at different stepping potentials with $[Co(bpy)_3]^{3+}$ in the electrolyte. The steady state current exhibits a sharp rise at a potential that corresponds to the $PMDI^{0/\bullet-}$ redox level.

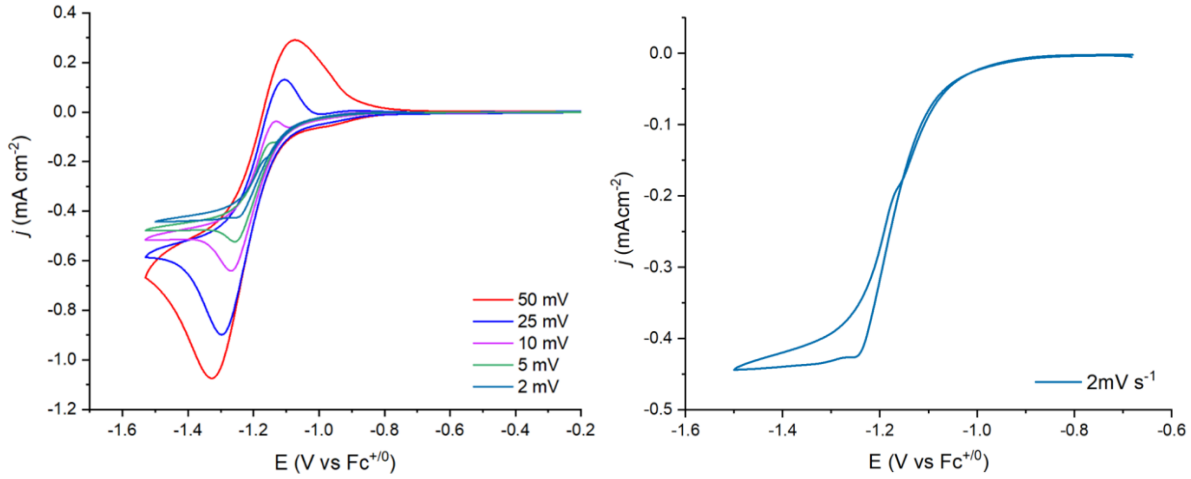

Figure S17. CVs of the FTO|Zn(PMDI)|Zn(NDI) bilayer electrode in the presence of the $[Co(bpy)_3]^{3+}$ electron acceptor. C^0_A = 36 mM at ν = 2 mV s^{-1} (cyan), 5mV s^{-1} (green), 10 mV s^{-1} (pink), 25mV s^{-1} (blue), and 50 mV s^{-1} (red) (left). The cathodic feature in the CV decreases with decreasing scan rate leading to a CV with a quasi-plateau current for ν = 2 mV s^{-1} (right). This behavior is consistent with electron transport through the entire bilayer electrode, and electron extraction by the $[Co(bpy)_3]^{3+}$ electron acceptor in the electrolyte.

Interfacial electron transfer reactions in the electrodes

Table S1. Electron transfer reactions at the FTO|Zn(PMDI)$_{0.5}$(NDI)$_{0.5}$ interface

	@FTO|Zn(PMDI)$_{0.5}$(NDI)$_{0.5}$ interface
Reduction process	$NDI + e^- \rightarrow NDI^{\cdot -}$
	$PMDI + e^- \rightarrow PMDI^{\cdot -}$
	$NDI^{\cdot -} + e^- \rightarrow NDI^{2-}$
	$PMDI^{\cdot -} + e^- \rightarrow PMDI^{2-}$
Oxidation process	$PMDI^{2-} - e^- \rightarrow PMDI^{\cdot -}$
	$NDI^{2-} - e^- \rightarrow NDI^{\cdot -}$
	$PMDI^{\cdot -} - e^- \rightarrow PMDI$
	$NDI^{\cdot -} - e^- \rightarrow NDI$

Table S2. Electron transfer reactions at the FTO-Zn(PMDI) interface and the Zn(PMDI)-Zn(NDI) interface

	@FTO|Zn(PMDI) interface	**@Zn(PMDI)|Zn(NDI) interface**
Reduction process	$PMDI + e^- \rightarrow PMDI^{\cdot -}$	$PMDI + e^- \rightarrow PMDI^{\cdot -}$ $PMDI^{\cdot -} + NDI \rightarrow PMDI + NDI^{\cdot -}$
	$PMDI^{\cdot -} + e^- \rightarrow PMDI^{2-}$	$PMDI^{\cdot -} + e^- \rightarrow PMDI^{2-}$ $PMDI^{2-} + NDI^{\cdot -} \rightarrow PMDI^{\cdot -} + NDI^{2-}$
Reoxidation process	$PMDI^{2-} - e^- \rightarrow PMDI^{\cdot -}$	$PMDI^{2-} - e^- \rightarrow PMDI^{\cdot -}$
	$PMDI^{\cdot -} - e^- \rightarrow PMDI$	$PMDI^{\cdot -} - e^- \rightarrow PMDI$ $PMDI + NDI^{2-} \rightarrow PMDI^{\cdot -} + NDI^{\cdot -}$

Table S3. Electron transfer reactions at the FTO-Zn(NDI) interface and the Zn(NDI)-Zn(PMDI) interface

	@FTO|Zn(NDI) interface	**@Zn(NDI)|Zn(PMDI) interface**
Reduction process	$NDI + e^- \rightarrow NDI^{\cdot -}$	$NDI + e^- \rightarrow NDI^{\cdot -}$
	$NDI^{\cdot -} + e^- \rightarrow NDI^{2-}$	$NDI^{\cdot -} + e^- \rightarrow NDI^{2-}$ $NDI^{2-} + PMDI \rightarrow NDI^{\cdot -} + PMDI^{\cdot -}$
Reoxidation process	$NDI^{2-} - e^- \rightarrow NDI^{\cdot -}$	$NDI^{2-} - e^- \rightarrow NDI^{\cdot -}$
	$NDI^{\cdot -} - e^- \rightarrow NDI$	$NDI^{\cdot -} - e^- \rightarrow NDI$ $NDI + PMDI^{\cdot -} \rightarrow NDI^{\cdot -} + PMDI$

References

(1) Kumar, A.; Li, J.; Inge, A. K.; Ott, S. Electrochromism in Isoreticular Metal–Organic Framework Thin Films with Record High Coloration Efficiency. *ACS Nano* **2023**, *17* (21), 21595-21603.